The *Proteus mirabilis rffG* gene is essential for swarm-associated cell elongation through an Rcs-mediated pathway

Kristin Little, Murray J. Tipping, and Karine A. Gibbs[#]

Department of Molecular and Cellular Biology, Harvard University, 16 Divinity Avenue

Cambridge MA, 02138, USA

Running head: *P. mirabilis* cell elongation requires the *rffG* gene

[#] Address correspondence to:

K. A. Gibbs, Ph.D.

Department of Molecular and Cellular Biology

Harvard University

16 Divinity Avenue

Cambridge, MA 02138

Ph: +1 617-496-1637

Em: *kagibbs@mcb.harvard.edu*

Keywords: RffG, Rcs phosphorelay, cell development, cell growth, outer membrane, cell differentiation, cell motility, bacterial genetics, stress response

Abstract

The gram-negative bacterium *Proteus mirabilis* can elongate up to 40-fold on surfaces before engaging in a social motility termed "swarming" that precedes division into short non-motile rod-shaped cells. The specific physical and genetic requirements for swarmer cell elongation are not fully understood. Here we further elucidate critical components for swarmer cell elongation. We show that the gene, *rffG,* is essential for cell envelope structure and integrity on a surface. The *rffG* gene encodes a predicted biosynthesis protein for the cell-envelope component, Enterobacterial Common Antigen. We observed that the production of large LPS-linked moieties requires the *rffG* gene; the chemical properties of these moieties remain unknown, but their loss corresponded with inhibition of swarmer cell elongation. We further show that inhibition of elongation occurs through the actions of the Rcs phosphorelay. The Rcs phosphorelay, which responds to cell envelope stress, is a known repressor of the master transcriptional regulator, $FlhD_4C_2$. Loss of *rffG* and the Rcs response regulator rescued motility but induced severe cell shape defects. These observations indicated that though swarmer motility and elongation into swarmer cells are genetically linked through Rcs, these are distinct processes during swarming. Building upon consensus models, we hypothesize that the Rcs phosphorelay in *P. mirabilis* functions as a developmental checkpoint to prevent cell envelope-compromised cells from initiating swarmer cell elongation and subsequent motility.

Importance statement

Proteus mirabilis is a primary cause of catheter-associated urinary tract infections, and its surface-based swarm motility has been implicated in virulence. Here we have characterized a

45 novel essentiality of the *rffG* gene in producing large LPS-linked moieties needed for cell
46 elongation, which in itself is a necessary first step of swarming. We have also elucidated a
47 previously undescribed role for the conserved Rcs stress response: retention of cell shape
48 separate from inhibition of the *flhDC* flagellar regulon. These data contribute to a broader
49 understanding of Rcs as a multifunctional regulator of cell integrity, motility, and virulence.

50 **Introduction**

51 Many bacteria move along a surface using a group motility termed swarming. For
52 *Proteus mirabilis*, a gram-negative commensal member of the human gut microbiome and
53 opportunistic pathogen, rapid surface based swarm motility likely contributes to its virulence
54 during catheter associated urinary tract infections (1, 2). *P. mirabilis* cells initiate a
55 developmental cell cycle upon surface growth. Cells elongate from 1-2 μm rods into hyper-
56 flagellated, snake-like "swarmer" cells that can range from 10 – 80 μm in length (3, 4). Swarmer
57 cells contain multiple chromosomes, are extensively flagellated, and closely associate into multi-
58 cell rafts that collectively move across a surface (3, 4). After a defined period of motility,
59 swarmer cells divide into short (1-2 μm) non-motile rod-shaped cells containing one
60 chromosome (5). Iterative rounds of swarmer cell elongation, group motility, and cell division
61 result in the rapid occupation of centimeter-scale surfaces in a stereotypical concentric ring
62 pattern (5). Elongation into swarmer cells is coordinated with changes to the cell envelope, most
63 notably in the alteration of outer membrane (OM) structure and properties: the
64 lipopolysaccharide (LPS) structure changes, OM fluidity increases, and areas of lipid bilayer
65 arise in the outer membrane (6-8). Cells also transition through unknown mechanisms from
66 being short and rigid to long and flexible with a phenotypic S-shaped curving (3, 4), suggesting
67 uncharacterized changes to cell wall structure may occur.

68 Cell envelope structure and stress sensing appear to play broadly conserved roles in
69 swarm regulation in several bacterial species, including *P. mirabilis*, *Escherichia coli*, and
70 *Serratia marcescens* (9-17). Interrogating the contribution of specific aspects of cell envelope
71 structure to cell elongation has proven challenging. The three broad cell envelope biosynthesis
72 pathways in Enterobacteriaceae produce LPS, Enterobacterial Common Antigen (ECA), and

73 peptidoglycan (PG) for the cell wall. In *E. coli*, genetic modifications to each of these
74 biosynthetic pathways can dramatically alter cell shape and motility due to perturbations in the
75 balance of cell envelope substrates that are shared between the pathways (12, 13). For example,
76 genetic deletion of specific LPS and ECA biosynthesis genes results in the accumulation of dead-
77 end intermediate products that sequester undecaprenyl phosphate (12, 13). In addition,
78 perturbation of cell wall biosynthesis and formation of inert peptidoglycan islands can lead to
79 cell division and branching defects in other bacterial species (18-21).

80 Strikingly, such defects are not observed in swarming *P. mirabilis* even though the cells
81 regularly oscillate between being short and rigid versus long and flexible. How *P. mirabilis* cells
82 can withstand regular dramatic changes in cell envelope structure during swarmer cell elongation
83 is not fully explained. For example, the effects of perturbing LPS or ECA biosynthesis in *P.*
84 *mirabilis* are not resolved. Disruption of LPS biosynthesis genes *waaL* (15, 22) or *ugd* (23)
85 inhibits swarmer cell elongation and motility through inhibition of surface sensing (22) and
86 activation of RpoE (16, 23), respectively. However, disruption of ECA ligation through deletion
87 of *wzyE* has minimal effects on *P. mirabilis* elongation or motility (22). In this paper, we address
88 whether disruption of the ECA biosynthesis pathway upstream of the *wzyE*-encoded ligase
89 affects swarming, and further, how cells respond to these cell envelope perturbations.

90 Across several bacterial species, the Rcs phosphorelay has been directly implicated in
91 swarm regulation; this phosphorelay functions by altering gene expression via the transcriptional
92 response regulator, RcsB (9, 10, 15, 24) (see also reviews (25, 26)). RcsB serves as a potent
93 inhibitor of swarmer cell elongation and motility by blocking expression of the genes *flhDC*,
94 which encode the master transcriptional regulator of swarming $FlhD_4C_2$ (10, 14). $FlhD_4C_2$ is an
95 early activator of flagellar gene expression in *P. mirabilis*, *E. coli*, and other bacteria species.

96 Release of Rcs inhibition is sufficient to drive swarmer cell development; RcsB-deficient *P.*
97 *mirabilis* cells constitutively elongate in liquid (14). Multiple cell envelope stresses, such as
98 perturbations to ECA or LPS, activate the Rcs response in several bacterial species (9, 15, 24).
99 Less clear is whether the Rcs response to cell envelope stress during swarming acts solely
100 through the *flhDC* regulon. The Rcs regulon in *P. mirabilis* was recently defined, and
101 intriguingly, RcsB directly modulates expression of cell division genes to regulate swarmer cell
102 development independently of $FlhD_4C_2$ (27, 28). This result is consistent with earlier findings in
103 *E. coli*: Rcs has conditional roles in *de novo* cell shape establishment (29). Therefore, we also
104 assessed whether the cell response to membrane perturbations proceeds simply and directly
105 through the predicted Rcs and $FlhD_4C_2$ pathways.
106 Here we present evidence that cell envelope integrity, produced in part by the *rffG* gene,
107 is essential for swarmer cell elongation and that Rcs is necessary for maintaining cell shape in
108 pathways separate from $FlhD_4C_2$-regulated elongation and motility. We show that *P. mirabilis*
109 cells require the ECA biosynthesis gene *rffG* to produce uncharacterized high molecular weight
110 (HMW) LPS-bound moieties. Loss of these moieties correlated with inhibition of swarmer cell
111 elongation through the Rcs phosphorelay and *flhDC*. Notably, we elucidated that the Rcs
112 response to cell envelope defects in *P. mirabilis* encompassed pathways separate from *flhDC*
113 through genetic analyses and gene expression profiling. We propose that the Rcs phosphorelay
114 serves as or functions within a developmental checkpoint for cells on swarm-permissive
115 surfaces. Further, we propose that disruptions in biosynthetic pathways resulting in compromised
116 cell envelopes activate the Rcs phosphorelay to mediate cell development on surfaces.
117
118 **Results**

119 **The *rffG* gene is essential for the production of LPS-associated OM moieties**

120 We examined the potential roles of less-studied OM components by targeting the ECA
121 biosynthesis gene, *rffG*, in wild-type *P. mirabilis* (WT). A homologous *rff* gene cluster is
122 responsible for ECA production in *E. coli* (30). We generated a deletion of the *rffG* gene, which
123 is predicted to encode a dTDP glucose-4,6-dehydratase; this mutant is hereafter called "Δ*rffG*".
124 We also complemented Δ*rffG* through expression of *rffG* under the *lac* promoter on a plasmid,
125 which constitutively expresses in *P. mirabilis* (22); this strain is hereafter called "*rffG*-
126 complemented."

127 Understanding of ECA state and localization in *P. mirabilis* is incomplete. ECA exists in
128 many forms: linked to other lipids, found in a circularized and soluble form, or surface-exposed
129 and linked to the LPS core (30-35). Therefore to characterize whether the loss of *rffG* alters OM
130 structures, we extracted LPS from surface-grown colonies of WT, Δ*rffG,* and *rffG*-complemented
131 populations and visualized the LPS-associated moieties using silver stain (36). The observed
132 banding patterns of the WT and *rffG*-complemented populations were nearly equivalent (Figure
133 1A). The banding pattern of the Δ*rffG* population, however, lacks a high molecular weight
134 (HMW) smear, and the bands within the putative O-antigen ladder formed doublets instead of
135 singlets (Figure 1A). We concluded that *rffG* is essential for production of wild-type O-antigen
136 and the HMW smear. We inferred that the HMW smear might consist of LPS-associated ECA
137 moieties based on the proposed function of *rffG* in the production of ECA. However, we are
138 conservatively referencing this smear as "HMW LPS-associated moieties" as opposed to "LPS-
139 linked ECA" because repeated efforts to confirm the presence of ECA via Western blotting with
140 *E. coli* O14 serum (reactive against ECA) (SSI Diagnostica, Hillerød, Denmark) (37, 38) were
141 unsuccessful.

142 We additionally predicted that these observed perturbations to the LPS components in the
143 Δ*rffG* cells likely cause broader cell envelope damage. We assessed cell viability and cell
144 envelope integrity to address whether Δ*rffG* cells might exhibit broad disruption of cell envelope
145 structure and/or integrity. We first measured the growth of WT, Δ*rffG*, and *rffG*-complemented
146 in nutrient-rich broth and on nutrient-rich agar. Growth in either condition was not impacted by
147 loss of the *rffG* gene (Figure SF1A, SF1B), though the colony size of Δ*rffG* was smaller when
148 grown on solid agar (Figure SF1C). We next used envelope-challenging conditions to probe the
149 integrity of the cell envelope. To target the OM, we measured resistance to Polymyxin B (PmB)
150 and bile salts. PmB is thought to act by targeting the LPS; disruption of LPS biosynthesis genes
151 induce PmB sensitivity in *P. mirabilis* (23, 39). Bile salts broadly target membranes through
152 detergent-like effects (40). ECA is likely involved in bile salts resistance of *Salmonella enterica*
153 (41); however, a role for ECA in bile salt resistance of *P. mirabilis* has not been explored. Both
154 WT and the Δ*rffG* strains were resistant to 50 mg/mL PmB (Figure SF1D), which approaches the
155 solubility of PmB in water. Both WT and Δ*rffG* populations grew on 0.1% bile salts and
156 exhibited decreased growth at 0.2% and 0.5% (Figure 1B). However, the growth defects of Δ*rffG*
157 populations on 0.2% were relatively more severe than those of WT cells; populations formed
158 small and translucent colonies (Figure S1B). Therefore, the Δ*rffG* populations exhibited growth
159 defects in the presence of bile salts as compared to WT, but not in PmB, indicating that the OM
160 integrity is compromised in the Δ*rffG* cells (Figure 1B).
161 To further interrogate cell envelope integrity, we analyzed cell morphology in response to
162 subclinical levels of carbenicillin (10 µg/ml Cb). WT cells lengthened to tens of microns after
163 two or four hours of Cb treatment, and the overall appearance was even in width with occasional
164 mid-cell bloating (Figure 1C); this observation is comparable to reports for *E. coli* and *P.*

165 *mirabilis* (42). Bloating became more pronounced after four hours of exposure, though little cell
166 lysis was observed. The Δ*rffG* cells exhibited cell shape defects after one hour of Cb exposure.
167 These defects became enhanced after two hours as cells elongated, and the majority of cells were
168 lysed after four hours on Cb (Figure 1C). Equivalent results were attained with Aztreonam, an
169 inhibitor of the cell division protein, FtsI (Figure SF1E). We deduced that *rffG*-deficient cells
170 were sensitized to cell wall stress and contained compromised cell envelopes, indicating that the
171 *rffG* gene is essential for wild-type cell envelope formation.
172
173 **Cells require *rffG* to complete swarmer cell elongation and initiate swarming**
174 As perturbations to LPS structure are known to inhibit swarm motility in *P. mirabilis*
175 (22), we predicted that *rffG*-deficient cells would be prohibited from swarming. We
176 characterized the swarm developmental cycle of WT, Δ*rffG,* and *rffG*-complemented
177 populations. Swarms of the WT population occupied a circle of 10-centimeter diameter on rich
178 media within 24 hours (Figure 2A). Under the same conditions, swarms of the Δ*rffG* population
179 did not expand beyond the inoculum, while swarms of the *rffG*-complemented populations
180 expanded roughly half the distance of WT and formed a restricted terrace structure (Figure 2A).
181 Hence, the *rffG* gene was necessary for swarm colony expansion; however, the native levels or
182 expression dynamics of *rffG* expression likely contribute to its activity.
183 It remained unclear at which stage of swarming the Δ*rffG* cells likely inhibited:
184 elongation and/or motility. We examined populations of WT, Δ*rffG*, and *rffG*-complemented
185 cells using epifluorescence microscopy under swarm-permissive conditions to assess cell
186 morphology. A fluorescent Venus reporter downstream of *fliA* was introduced on the
187 chromosomes of each strain background to visualize flagellar gene expression across each

188 population. The *fliA* gene is directly regulated by $FlhD_4C_2$ and is highly expressed in swarming
189 cells (43, 44). By four hours after inoculation, WT populations comprised both short non-motile
190 and elongated motile cells, demonstrating that cells progressed normally through the swarm cell
191 cycle. Populations became enriched in elongated cells that brightly expressed the *fliA* reporter by
192 six hours (Figure 2C). These observations confirm previous observations that expression of
193 flagellar genes occurs in a time-dependent manner on surfaces (22). By contrast, most Δ*rffG* cells
194 at four and six hours were short, non-motile, and at six hours largely did not exhibit *fliA* reporter-
195 induced fluorescence (Figure 2C). A subset of Δ*rffG* cells did appear to initiate elongation
196 (Figure 2C) but often lysed or divided into short cells (Figure SF2). The *rffG*-complemented
197 cells formed elongated motile cells with *fliA* reporter fluorescence comparable to WT by six
198 hours, though this progression was delayed compared to WT cells (Figure 2C). Altogether, these
199 observations indicated that *rffG* is necessary for cells to exhibit two hallmarks of swarmer cell
200 development: cell elongation and flagellar gene expression. We concluded that the impaired
201 swarm motility was because *rffG*-deficient cells are unable to elongate into swarmer cells.
202

203 ***rffG*-deficient cells have a gene expression profile distinct from that of WT**

204 Inhibition of swarm elongation in *rffG*-deficient cells could be achieved via a physical
205 defect of the cell membrane or via activation of an inhibitory signaling cascade upstream of
206 known swarm-promoting factors. LPS deficiencies initiate signaling via the Rcs phosphorelay
207 and suppress swarming via RcsB inhibition of *flhDC* expression (15). To resolve how swarmer
208 cell elongation is inhibited in *rffG*-deficient cells, we performed two rounds of RNA-Seq
209 analysis on WT and Δ*rffG* populations grown in swarm-permissive conditions so that we could
210 identify pathways disrupted in the Δ*rffG* background. As there are known transcriptional

211 differences between non-motile and actively swarming cells (44), we used short, non-motile WT
212 cells harvested from swarms.

213 We stringently considered "significant" any expression levels which were at least four-
214 fold divergent from that of WT. Of ~ 3500 genes in the *P. mirabilis* genome, 207 genes were
215 significantly increased in Δ*rffG* as compared to WT (Table S1, Figure 3A), and of these genes,
216 about a third could not be assigned a function (Figure 3B). Notably, expression of 29 fimbria or
217 adhesion related genes was increased; these genes included the virulence-associated MR/P
218 fimbrial operon (200-fold increased expression of *mrpA*) and *pmpA* (*Proteus* P-like pili, 55.5-
219 fold increased) (Table 1, Table S1). Several genes related to carnitine metabolism (the
220 transcriptional regulator *caiF* at 63.6-fold and *caiA, fixC,* and *fixX* at four-fold), as well as genes
221 related to the TCA cycle and oxidative phosphorylation were also up-regulated, including
222 *frdABCD* (4-8 fold increased) and *cydAB* (4-6-fold increased) (Tables 1, Table S1). Carnitine can
223 be metabolized under aerobic conditions for *Proteus*, but the greatest metabolism occurs under
224 anaerobic conditions (45, 46). Carnitine metabolism is a nutrient source as well as a stress
225 protectant for several bacterial species (47-49). Likewise, *ompW* was increased ~ 33.7 fold along
226 with *dcuB*, an anaerobic C4-dicarboxylate transporter, at 29.6 fold (Table 1, Table S1). In *E. coli*,
227 maximal *ompW* expression is tied to survival in the transition from aerobic to anaerobic growth
228 (50). In summary, the Δ*rffG* cells have upregulated genes for fimbrial production and for
229 metabolism under anaerobic or micro-aerobic environments.

230 Conversely, we observed decreased expression of 136 genes in the Δ*rffG* populations
231 relative to WT (Table S2, Figure 3A), of which approximately a third could not be assigned a
232 function (Figure 3B). 20% of the down-regulated genes were directly related to flagella assembly
233 or chemotaxis (Tables 2, Table S2). In addition, factors known to promote swarmer cell

234 development and motility also had decreased expression, including *umoD* at 0.12-fold, *umoA* at
235 0.19-fold expressed, and *ccm* at 0.12-fold expressed (Table 2). Another approximately 18% of
236 the down-regulated genes were related to ribosome structure and translation (Figure 3B).
237 Additionally, three key regulators linked to stress or fimbrial production were differentially
238 regulated: *mrpJ* (19.1-fold increased) (51), *rpoS* (8.7-fold increased), and the RcsB-cofactor *rcsA*
239 (9.9-fold increased) (27, 28). Interestingly, we observed partial overlap between the genes
240 differentially regulated in Δ*rffG* and the recently characterized regulon of RcsB in *P. mirabilis*
241 (27, 28) (Figure 3A). The overlap was especially significant amongst down-regulated genes
242 (Figure 3A). RcsB negatively regulates the *flhDC* regulon (flagella and chemotaxis genes) and
243 positively regulates the *mrpJ* gene (27, 28). We hypothesized that the Rcs phosphorelay was
244 active in the Δ*rffG* population given this expression profile.
245
246 ***flhDC and RcsB respond to* Δ*rffG*-associated cell elongation and swarm defects**
247 Based on a consensus model derived from previous research (15, 24, 52), we posited that
248 Δ*rffG*-associated cell envelope defects likely initiate the Rcs phosphorelay to subsequently
249 inhibit *flhDC* expression. To interrogate this model for the *rffG*-deficiency, we utilized the fact
250 that *flhDC* overexpression in wild-type *P. mirabilis* drives elongation of swarmer cells (53). The
251 resultant swarm colony forms a thin film without a concentric ring pattern, termed a
252 "hyperswarming" phenotype (14). We overexpressed *flhDC* in the WT and Δ*rffG* strain
253 backgrounds, resulting in WT + *flhDC* and Δ*rffG* + *flhDC*, respectively; swarm colonies of the
254 resultant strains both exhibited hyperswarming (Figure SF3A). We also observed these
255 populations by epifluorescence light microscopy using strains in which the *fliA*-venus
256 transcriptional reporter had been introduced. After six hours of growth on a swarm permissive

257 surface, both WT + *flhDC* and Δ*rffG* + *flhDC* populations were comprised of motile, elongated
258 cells with comparable fluorescence due to the *fliA* reporter (Figure 4A-B). We considered that
259 the swarming recovery in the *flhDC* overexpression strains might be due to restoration of the
260 HMW LPS-associated moieties. We analyzed the LPS fractions of Δ*rffG* + *flhDC* cells and
261 observed that the HMW LPS-associated moieties remained absent (Figure SF3B). Therefore,
262 over-expression of *flhDC* was not sufficient to restore production of this OM component (Figure
263 SF3B), which in itself indicates that this *rffG*-generated HMW OM component is not physically
264 required for swarmer cell elongation and motility. We further concluded that increased
265 expression of *flhDC* is sufficient to restore swarmer cell elongation, flagellar gene expression,
266 and motility to Δ*rffG* cells independently of OM structure.

267 These results confirmed that the inhibition of elongation in Δ*rffG* cells is due to a
268 signaling cascade. As RcsB acts upstream of *flhDC*, we hypothesized that deletion of *rcsB* would
269 also rescue swarmer cell elongation and motility, resulting in a phenotype equivalent to that of
270 the *flhDC* overexpression strains. However, direct comparisons of *flhDC* overexpression and
271 *rcsB* deletion are not readily apparent in the literature. We generated chromosomal deletions of
272 *rcsB* in the WT and Δ*rffG* strain backgrounds, resulting in Δ*rcsB* and Δ*rffG*Δ*rcsB*, respectively.
273 We confirmed that deletion of *rcsB* did not rescue the LPS-associated defects of Δ*rffG* (Figure
274 SF3B) and then tested the ability of these populations to engage in swarm motility. The Δ*rcsB*
275 populations formed hyperswarming colonies that covered a 10-cm surface in 24 hours (Figure
276 SF3C), which is consistent with previous reports (14). Surprisingly, swarm colonies of the
277 Δ*rffG*Δ*rcsB* population appeared mucoid with tight concentric swarm rings and expanded to less
278 than half the distance of the WT population (Figure SF3C), indicating that the Δ*rffG*Δ*rcsB* were
279 not fully rescued for swarm motility. To further characterize this swarming defect, we examined

280 Δ*rcsB* and Δ*rffG*Δ*rcsB* strains encoding the *fliA*-Venus transcriptional reporter by
281 epifluorescence light microscopy after six hours of growth on a swarm permissive surface. Cells
282 in the Δ*rcsB* populations were generally elongated and motile with increased fluorescence
283 expression, similar to cells of the WT + *flhDC* population (Figure 4C). Cells in the Δ*rffG*Δ*rcsB*
284 population, however, exhibited striking cell shape defects; cells were bloated, uneven in width,
285 formed spheres or tapering at the cell poles, or bulged at the mid-cell (Figure 4D). In addition,
286 several Δ*rffG*Δ*rcsB* cells were forked at the cell pole or branched at the mid-cell (Figure 4D).
287 The elongated cells in the Δ*rffG*Δ*rcsB* population also exhibited fluorescence, indicating that *fliA*
288 expression was restored, and cells engaged in swarm motility (Figure 4D). Altogether, loss of
289 *rcsB* was sufficient to partially restore swarmer cell elongation and motility to Δ*rffG* cells.
290 However, RcsB was also necessary for maintenance of proper cell shape in these envelope-
291 compromised cells.
292
293 **Discussion**
294 This research provides initial evidence that deletion of *rffG*, a predicted ECA
295 biosynthesis gene, inhibits *P. mirabilis* swarmer cell elongation. These results add to a growing
296 understanding of the importance of cell envelope composition to *P. mirabilis* swarming and
297 expands upon previous studies showing that OM structure directly regulates early stages of
298 swarmer cell development. Abrogation of O-antigen structure through deletion of the O-antigen
299 ligase (*waaL*) or chain length determinant (*wzz*) inhibits surface sensing, the earliest stage in the
300 swarmer cell cycle (22). The authors proposed that O-antigen mechanically senses the surface
301 and communicates this information via the Umo system (15). Here we propose that *P. mirabilis*
302 cells likely require additional cell envelope structures for swarmer cell elongation and possibly

303 surface sensing. Loss of *rffG* leads to an altered profile for LPS-linked moieties; cells lacked
304 uncharacterized HMW LPS-linked moieties and appeared to assemble a modified O-antigen
305 ladder. Based on the proposed function of the *rffG* gene product, we hypothesize that the HMW
306 LPS-linked moieties may be ECA or ECA-derived. However, efforts to confirm the presence of
307 LPS-linked ECA in *P. mirabilis* strain BB2000 have been unsuccessful to date, and further work
308 must be done to characterize the structural changes to the LPS. Regardless, this research supports
309 that the *rffG* gene is critical for the production of cell envelope components necessary for
310 swarming.

311 In addition to changes in OM structure, we also observed that *rffG*-deficient cells were
312 more susceptible to cell envelope stress. While *rffG* has been linked to ECA production, this
313 result suggests that deletion of *rffG* leads to pleiotropic effects impacting overall cell envelope
314 integrity. This is not surprising as perturbation of ECA or LPS biosynthesis genes result in the
315 accumulation of dead-end intermediates that broadly impact cell envelope integrity in *E. coli* (12,
316 13). Peptidoglycan, LPS, and ECA biosynthesis pathways share substrates, such as undecaprenyl
317 phosphate or lipid I (12, 13). Perturbation of the flux or sequestration of these shared substrates
318 across pathways broadly impact cell envelope integrity and can result in shape defects (12, 13).
319 Furthermore, previous work suggests that OM structure plays a crucial mechanical role in
320 resisting turgor pressure fluctuations associated with cell wall stressors, specifically beta-lactam
321 drugs (54). However, it remains unclear whether loss of the HMW LPS-linked moieties results in
322 compromised OM integrity and if such OM defects alone are sufficient to sensitize *rffG*-deficient
323 *P. mirabilis* cells to shape defects. Intriguingly, shape defects were not apparent in *rffG*-deficient
324 cells except for the subset of cells that undergo elongation on surfaces. It remains unclear why a
325 subpopulation of Δ*rffG* cells escape inhibition of elongation, or how factors leading to this

326 escape might contribute to cell shape. Additionally, loss of *rffG* resulted in broad changes to the
327 *P. mirabilis* transcriptome on surfaces. These changes included increased production of several
328 fimbrial gene clusters in concert with repression of flagellar and chemotaxis genes, along with
329 altered expression of several metabolism genes. Several defense-associated genes and stress-
330 associated transcription factors (*rcsA* and *rpoS*) were also up-regulated, suggesting the cells may
331 be activating stress-related pathways. We surmise that *rffG*-deficient cells enter into a
332 transcriptional state distinct from that of the swarm cycle; it is unclear whether this lifestyle
333 would persist for disruptions in other cell envelope biosynthesis pathways.

334 While several genetic pathways were perturbed, a central cell response through the Rcs
335 phosphorelay and *flhDC* appeared to be sufficient to restrict initiation of swarmer cell
336 development. Yet remarkably, we found that overexpression of *flhDC* and deletion of *rcsB* in
337 *rffG*-deficient cells did not result in the same phenotype; concurrent removal of *rcsB* and *rffG*
338 caused shape defects among swarming cells. These shape defects were not observed in Δ*rffG*
339 cells over-expressing *flhDC,* suggesting that neither expression of *flhDC* or elongation are
340 sufficient to induce shape defects. These observations support a novel role for Rcs in maintaining
341 the fidelity of the rod shape during swarmer cell elongation. As cells with intact cell envelopes
342 appear to have no requirement for *rcsB* to maintain shape, we surmise that a function for RcsB in
343 maintaining cell shape might be limited to cells with compromised envelopes. In fact, the Rcs
344 phosphorelay was recently proposed to act as a multifunctional regulator of swarmer cell
345 development through distinct modulation of motility and cell division regulators (27, 28). Our
346 results expand an understanding of the important and complex role that the Rcs phosphorelay has
347 in swarmer cell development and motility.

348 Remaining unclear is why constitutive expression of *flhDC* was sufficient to restore
349 swarmer cell elongation to Δ*rffG* cells while maintaining cell shape and polarity. Based on the
350 fact that the Rcs phosphorelay responds to cell stress, we predict that RcsB may play a role in
351 maintaining cell envelope integrity through unknown mechanisms in these *flhDC*-overexpression
352 cells. If so, constitutive expression of *flhDC* under a non-native promoter likely uncoupled the
353 *flhDC*-repressive and cell envelope protective activities of RcsB. Thus, Δ*rffG* + *flhDC* cells may
354 represent an artificial system in which cells are driven to elongate while maintaining the cell
355 envelope protective effects of Rcs activation (Figure 5). As such, we deduce that the cell shape
356 protective effects of RcsB occur upstream of *flhDC.* Thus, this work reveals a previously
357 underappreciated *flhDC*-independent pathway linking RcsB to swarmer cell elongation.
358 Others have also proposed that Rcs plays a conditional role in cell shape maintenance in
359 gram-negative bacteria. L-form *E. coli* cells require the Rcs stress response to recover a rod
360 shape; cells lacking this response lyse (29). The authors of that study proposed that Rcs may
361 function to maintain cell shape in conditions in which cells may lose cell wall through exposure
362 to lysozyme or cationic antimicrobial peptides, including several niches within a human host
363 (29). In addition to overall bloating and irregularity of width, cells lacking both *rffG* and *rcsB*
364 cells exhibited perturbation of cell pole structure and growth from the mid-cell. To our
365 knowledge, we are the first to describe such defects in *P. mirabilis.* However, similar phenotypes
366 have been described in *E. coli* and *Agrobacterium tumerfaciens.* In those organisms, cell polarity
367 defects appeared to arise from the formation of patches of inert peptidoglycan and mislocalized
368 division planes (18-21, 55). Further study is needed to mechanistically understand which aspects
369 of the RcsB regulon are specific for cell shape maintenance.

370 Several questions also remain regarding the mechanism of activation and the downstream
371 activity of RcsB in *rffG*-deficient cells. First, Bode et al recently demonstrated that MrpJ also
372 acts as a regulator toggling cells between swarm motility (MrpJ-repressed) and non-motile
373 adherence (MrpJ-induced) (51); RcsB positively regulates MrpJ (27, 28). However, the genes
374 differentially regulated in Δ*rffG* (Table S1, S2) neither fully overlap with the RcsB regulon (27,
375 28) or the MrpJ regulon (51). Clearly additional pathways are affected in the *rffG*-deficient cells;
376 one such candidate is the RpoE regulon (16). And pathways connecting RcsB and MrpJ to
377 swarmer cell elongation and *flhDC*-dependent motility need to be more fully characterized.
378 Second, perturbation of OM structure appears to be communicated through both RcsF-dependent
379 and independent pathways in *P. mirabilis* (15). It remains unclear whether cell envelope stress of
380 the *rffG*-deficient cells is communicated through the OM-localized RcsF, through the
381 upregulation of RcsA, or through an uncharacterized additional pathway. Also unknown is
382 whether the *rffG*-dependent HMW LPS-linked moieties act through the Umo system, as was
383 previously shown for O-antigen (15). Finally, the DNA-binding activity of RcsB has been shown
384 to be modulated by both phosphorylation and association with auxiliary transcription factors in
385 *E. coli* (56). How RcsB activity is modulated downstream of phosphorylation remains unclear in
386 *P. mirabilis.*
387 Taken together with recent research on the Rcs regulon in *P. mirabilis* (27, 28), we
388 propose that the Rcs phosphorelay functions as a developmental checkpoint for the swarm cell
389 cycle (Figure 5). Under swarm-friendly conditions in the presence of wild-type cell envelope
390 structure, Rcs would be inactive thereby allowing the swarm cell cycle to progress. By contrast,
391 the absence or alteration of the cell envelope structure likely activates the Rcs phosphorelay,
392 which in turn a) activates pathways protective against cell shape defects, b) activates cell

393 division pathways, and c) inhibits expression of *flhDC*. Based on the transcriptional profile of
394 Δ*rffG* cells and other cells activating the Rcs phosphorelay (27, 28), we predict that the activity
395 of Rcs culminates in the adaptation of an adherent or biofilm-promoting lifestyle that may
396 provide protection against external stressors. We propose that the HMW LPS-linked moieties,
397 which are potentially ECA, might provide one important signal that communicates cell integrity
398 to the Rcs system. As many species within the Enterobacteriaceae family express both ECA and
399 the Rcs phosphorelay, ECA and Rcs might serve as broad-acting regulators of bacterial cell
400 development and motility.
401
402
403 **Experimental Procedures**
404 Growth conditions
405 Liquid cultures were grown in LB-Lennox broth. Colonies were grown in 0.3 % LB agar for
406 swimming motility assays, on LSW- agar (57) for plating non-motile colonies, and on CM55
407 blood agar base (Oxoid, Hampshire, UK) for swarming. Antibiotics for selection were used
408 throughout all assays as following: 15 µg/mL tetracycline, 25 µg/mL streptomycin, and 35
409 µg/mL kanamycin. For swarm assays, overnight cultures were normalized to OD_{600} 1.0, and 1 µl
410 of culture was inoculated with a needle onto swarm-permissive CM55 blood agar base plates
411 containing kanamycin, 40 µg/mL Congo Red, and 20 µg/mL Coomassie Blue. Plates were
412 incubated at 37 °C. For swim assays, an inoculation needle was used to inoculate overnight
413 cultures into 0.3% LB containing kanamycin. Plates were incubated at 37 °C for 16 hours.
414 Images were taken with a Canon EOS 60D camera.
415

416 Strain construction

417 Strain construction was performed as described previously (58). For construction of the Δ*rcsB*
418 strain, a gBlock (Integrated DNA Technologies, Coralville, IA) containing the 452 base-pairs
419 (bp) upstream and downstream of *rcsB* (*P. mirabilis* BB2000, accession number CP004022:nt
420 1972701…1973153 and 1973809…1974261) was generated and introduced to pKNG101 at SpeI
421 and XmaI sites using Slice cloning (59). Similarly, for construction of the Δ*rffG* strain, a gBlock
422 containing a chloramphenicol resistance cassette (amplified from pBAD33 (60)) flanked by 1000
423 bp upstream of *rffG* and downstream of *rffG* (*P. mirabilis* BB2000, accession number
424 CP004022:nt 3635400…3636399 and 3637473…3638473) was introduced to pKNG101 (58) at
425 the same sites. Expression plasmids were introduced into *P. mirabilis* via *E. coli* SM10lpir as
426 previously described (57). Resultant strains were confirmed by Polymerase Chain Reaction
427 (PCR) of the targeted region. The Δ*rffG* strain was confirmed through whole genome sequencing
428 as described in (61).

429

430 For construction of *fliA* reporter strain, a gBlock encoding the last 500 bp *fliA* (*P. mirabilis*
431 BB2000, accession number CP004022:nt 1856328…1856828), RBS (aggagg), a modified
432 variant of Venus fluorescent protein (a gift from Drs. Enrique Balleza and Phillipe Cluzel), and
433 500bp downstream *fliA* (*P. mirabilis* BB2000, accession number CP004022:nt
434 1855828…1856328) was inserted into pKNG101 (58) at the ApaI and XbaI sites. Expression
435 plasmids were introduced into *P. mirabilis* via *E. coli* SM10lpir as previously described (57).
436 Resultant strains were confirmed by PCR of the targeted region and sequenced.

437

438 For construction of the *rffG* expression strains, the nucleotide sequence for *rffG* was PCR
439 amplified from the *P. mirabilis* chromosome using oKL273 and oKL274 and inserted into
440 expression vector pBBR1-NheI (62) using AgeI and NheI restriction enzyme sites. For the *flhDC*
441 expression strains, the nucleotide sequences *flhDC* (amplified using oKL277 and oKL278) was
442 similarly inserted into pBBR1-NheI. A gBlock containing the *lac* promoter (sequence:
443 cacggtcacactgcttccggtagtcaataaaccggtgcgcaacgcaattaatgtgagttagctcactcattaggcaccccaggctttacacttt
444 atgcttccggctcgtatgttgtgtggaattgtgagcggataacaatttcacacaggaaacagctatgaccatgattacgaaggatcctaggag
445 gtactagtatg) was introduced upstream of the coding region using Slice (59). Plasmids were
446 confirmed by Sanger Sequencing (Genewiz, South Plainfield, NJ). Expression plasmids were
447 introduced into *P. mirabilis* via *E. coli* S17lpir as previously described (57).
448
449 LPS extraction and analysis
450 Cells were grown on overnight at 37°C on swarm-permissive agar and harvested with LB. LPS
451 from cells was extracted using an LPS Extraction Kit according to manufacturer's instructions
452 (iNtRON Biotechnology Inc, Sangdaewon Seongnam, Gyeonggi, Korea). Extracts were
453 resuspended in 10mM Tris, pH 8.0 buffer and run on a 12% SDS-PAGE gel. Gels were stained
454 with a modified silver stain protocol (36).
455
456 Bile salts resistance assays
457 Cultures were grown overnight, normalized to OD 1.0, and serial diluted 10-fold. 1 µL spots of
458 10^{-1} to 10^{-8} dilutions of each strain (in technical triplicate) were inoculated onto LSW- plates
459 containing bile salts (filter sterile, added to medium post-autoclaving). Plates were incubated
460 overnight at 37°C.

461

462 Carbenicillin sensitivity assay

463 Cells were harvested from swarm permissive medium using LB broth and spread onto 1 mm agar
464 pads containing swarm permissive medium with 10 µg/mL carbenicillin (Corning, Corning,
465 NY). Cells were imaged after 1, 2, or 4 hours on surface. Three biological replicates were
466 analyzed.

467

468 Microscopy

469 Microscopy was performed as previously described (61). Briefly, swarm-permissive agar pads,
470 supplemented with 35 µg/mL kanamycin for plasmid retention, were inoculated from overnight
471 stationary cultures and incubated at 37°C in a modified humidity chamber. Pads were imaged
472 using a Leica DM5500B (Leica Microsystems, Buffalo Grove, IL) and a CoolSnap HQ2 cooled
473 CCD camera (Photometrics, Tuscon, AZ). MetaMorph version 7.8.0.0 (Molecular Devices,
474 Sunnyvale, CA) was used for image acquisition. Images were analyzed using FIJI (63) (National
475 Institutes of Health, USA); where indicated, images were subjected to background subtraction
476 (equally across entire image). Where indicated, cells were stained with 25 µM TMA-DPH
477 (Invitrogen, Carlsbad, CA), (max excitation 355 nm; max emission 430 nm) imaged in the DAPI
478 channel using an A4 filter cube (excitation 360/40 nm; emission 470/40 nm) (Leica
479 Microsystems, Buffalo Grove, IL). Venus (max excitation 515 nm; max emission 528 nm) was
480 visualized in the GFP channel using a GFP ET filter cube (excitation 470/40 nm; emission
481 525/50 nm) (Leica Microsystems, Buffalo Grove, IL). Fluorescence intensity and exposure times
482 for each fluorescence channel were equivalent across all fluorescence microscopy experiments.

483 Fluorescence due to Venus was not quantified and was visible due to the overlapping excitation
484 and emission spectra with the GFP ET filter cube.
485
486 Transcriptional analysis

487 Strains were grown on swarm-permissive agar plates at 37 ˚C. For WT samples, colonies were
488 inoculated on swarm-permissive agar and incubated overnight for swarm development. The
489 presence of short, non-motile cells in consolidation phase was confirmed by light microscopy.
490 Cells from the swarm edge were then harvested by scraping with a plastic loop into 1 ml of RNA
491 Protect solution (Qiagen, Venlo, Netherlands). The Δ*rffG* samples were harvested after overnight
492 incubation on swarm-permissive agar by scraping whole colonies into 1 ml RNA Protect
493 solution. Total RNA was isolated using an RNeasy Mini kit (Qiagen, Venlo, Netherlands)
494 according to the manufacturer's instructions. RNA purity was measured using an Agilent 2200
495 Tapestation (Agilent, Santa Clara, CA). To enrich mRNA, rRNA was digested using terminator
496 5' phosphate dependent exonuclease (Illumina, San Diego, CA) according to the manufacturer's
497 instructions and purified by phenol-chloroform extraction (64). cDNA libraries were prepared
498 from mRNA-enriched RNA samples using an NEBNext Ultra RNA library prep kit (New
499 England Biolabs, Ipswich, MA) according to the manufacturer's instructions. Libraries were
500 sequenced on an Illumina NextSeq 2500 instrument with 250-basepair single-end reads.
501 Sequences were matched to the BB2000 reference genome (accession number CP004022) using
502 Tophat 2 (65). Differential expression data were generated using the Cufflinks RNA-Seq
503 analysis suite (66) run on the Harvard Odyssey cluster, courtesy of the Research Computing
504 Group. Data were analyzed using the CummeRbund package for R and Microsoft Excel (66).
505 Gene functions were ascribed based on COG annotations (67). Bioinformatics information was

506 derived from KEGG (68). The data in this paper represent the combined analysis of two
507 independent biological repeats.
508
509 **Acknowledgements**
510 We would like to thank Drs. Enrique Balleza and Phillipe Cluzel for the kind gift of the Venus
511 construct and members of the Gibbs, D'Souza, Gaudet, and Losick labs for thoughtful discussion
512 and feedback. Drs. Doug Richardson, Sven Terclavers, and Sebastian Gliem assisted with
513 imaging on the Cell Observer. This research was funded by a Smith Family Fellowship in
514 Science and Engineering (KL), a Simmons Family Award for the Harvard Center for Biological
515 Imaging (KL) and by the David and Lucile Packard Foundation (KAG), the Merck Family Fund
516 (KAG), and Harvard University.
517
518 **Conflicts of Interest**
519 The authors declare no conflicts of interest.
520
521 **Author Contributions**
522 KL and KAG conceived and coordinated the study and wrote the paper. KL and KAG designed
523 all experiments; MJT performed RNA-Seq (Figure 3; Table 1, 2, S1, S2). KL all other
524 experiments. All authors edited the paper and approved the final version.
525
526

527 **References**

528 1. **Armbruster CE**, **Forsyth-DeOrnellas V**, **Johnson AO**, **Smith SN**, **Zhao L**, **Wu W**,
529 **Mobley HLT**. 2017. Genome-wide transposon mutagenesis of *Proteus mirabilis*:
530 Essential genes, fitness factors for catheter-associated urinary tract infection, and the
531 impact of polymicrobial infection on fitness requirements. PLoS Pathog **13**:e1006434.

532 2. **Burall LS**, **Harro JM**, **Li X**, **Lockatell CV**, **Himpsl SD**, **Hebel JR**, **Johnson DE**,
533 **Mobley HLT**. 2004. *Proteus mirabilis* genes that contribute to pathogenesis of urinary
534 tract infection: Identification of 25 signature-tagged mutants attenuated at least 100-fold.
535 Infect Immun **72**:2922–2938.

536 3. **Hoeniger J**. 1965. Development of flagella by *Proteus mirabilis*. Microbiology **40**:29–42.

537 4. **Hauser G**. 1885. Ueber Fäulnissbacterien und deren Beziehungen zur Septicämie: Ein
538 Beitrag zur Morphologie der Spaltpilze.

539 5. **Rauprich O**, **Matsushita M**, **Weijer CJ**, **Siegert F**, **Esipov SE**, **Shapiro JA**. 1996.
540 Periodic phenomena in *Proteus mirabilis* swarm colony development. J Bacteriol
541 **178**:6525–6538.

542 6. **Armitage JP**, **Smith DG**, **Rowbury RJ**. 1979. Alterations in the cell envelope
543 composition of *Proteus mirabilis* during the development of swarmer cells. Biochim
544 Biophys Acta **584**:389–397.

545 7. **Armitage JP**. 1982. Changes in the organization of the outer membrane of *Proteus*
546 *mirabilis* during swarming: freeze-fracture structure and membrane fluidity analysis. J
547 Bacteriol **150**:900–904.

548 8. **Gué M**, **Dupont V**, **Dufour A**, **Sire O**. 2001. Bacterial swarming: a biochemical time-
549 resolved FTIR-ATR study of *Proteus mirabilis* swarm-cell differentiation. Biochemistry
550 **40**:11938–11945.

551 9. **Castelli ME**, **Véscovi EG**. 2011. The Rcs signal transduction pathway is triggered by
552 enterobacterial common antigen structure alterations in *Serratia marcescens*. J Bacteriol
553 **193**:63–74.

554 10. **Francez-Charlot A**, **Laugel B**, **Van Gemert A**, **Dubarry N**, **Wiorowski F**, **Castanié-**
555 **Cornet M-P**, **Gutierrez C**, **Cam K**. 2004. RcsCDB His-Asp phosphorelay system
556 negatively regulates the *flhDC* operon in *Escherichia coli*. Molecular Microbiology
557 **49**:823–832.

558 11. **Toguchi A**, **Siano M**, **Burkart M**, **Harshey RM**. 2000. Genetics of swarming motility in
559 *Salmonella enterica* serovar typhimurium: critical role for lipopolysaccharide. J Bacteriol
560 **182**:6308–6321.

561 12. **Jorgenson MA**, **Young KD**. 2016. Interrupting biosynthesis of O antigen or the
562 lipopolysaccharide core produces morphological defects in *Escherichia coli* by

563 sequestering undecaprenyl phosphate. J Bacteriol **198**:3070–3079.

564 13. **Jorgenson MA**, **Kannan S**, **Laubacher ME**, **Young KD**. 2016. Dead-end intermediates
565 in the enterobacterial common antigen pathway induce morphological defects in
566 *Escherichia coli* by competing for undecaprenyl phosphate. Molecular Microbiology
567 **100**:1–14.

568 14. **Clemmer KM**, **Rather PN**. 2007. Regulation of *flhDC* expression in *Proteus mirabilis*.
569 Research in Microbiology **158**:295–302.

570 15. **Morgenstein RM**, **Rather PN**. 2012. Role of the Umo proteins and the Rcs phosphorelay
571 in the swarming motility of the wild type and an O-antigen (*waaL*) mutant of *Proteus*
572 *mirabilis*. J Bacteriol **194**:669–676.

573 16. **Liu M-C**, **Kuo K-T**, **Chien H-F**, **Tsai Y-L**, **Liaw S-J**. 2015. New aspects of RpoE in
574 uropathogenic *Proteus mirabilis*. Infect Immun **83**:966–977.

575 17. **Wang WB**, **Chen I-C**, **Jiang SS**, **Chen HR**, **Hsu CY**, **Hsueh PR**, **Hsu WB**, **Liaw SJ**.
576 2008. Role of RppA in the regulation of Polymyxin B susceptibility, swarming, and
577 virulence factor expression in *Proteus mirabilis*. Infect Immun **76**:2051–2062.

578 18. **Anderson-Furgeson JC**, **Zupan JR**, **Grangeon R**, **Zambryski PC**. 2016. Loss of PodJ
579 in *Agrobacterium tumefaciens* leads to ectopic polar growth, branching, and reduced cell
580 division. J Bacteriol **198**:1883–1891.

581 19. **Nilsen T**, **Ghosh AS**, **Goldberg MB**, **Young KD**. 2004. Branching sites and
582 morphological abnormalities behave as ectopic poles in shape-defective *Escherichia coli*.
583 Molecular Microbiology **52**:1045–1054.

584 20. **de Pedro MA**, **Young KD**, **Höltje J-V**, **Schwarz H**. 2003. Branching of *Escherichia coli*
585 cells arises from multiple sites of inert peptidoglycan. J Bacteriol **185**:1147–1152.

586 21. **Potluri L-P**, **de Pedro MA**, **Young KD**. 2012. *Escherichia coli* low-molecular-weight
587 penicillin-binding proteins help orient septal FtsZ, and their absence leads to asymmetric
588 cell division and branching. Molecular Microbiology **84**:203–224.

589 22. **Morgenstein RM**, **Clemmer KM**, **Rather PN**. 2010. Loss of the *waaL* O-antigen ligase
590 prevents surface activation of the flagellar gene cascade in *Proteus mirabilis*. J Bacteriol
591 **192**:3213–3221.

592 23. **Jiang SS**, **Lin TY**, **Wang WB**, **Liu MC**, **Hsueh PR**, **Liaw SJ**. 2010. Characterization of
593 UDP-glucose dehydrogenase and UDP-glucose pyrophosphorylase mutants of *Proteus*
594 *mirabilis*: Defectiveness in Polymyxin B resistance, swarming, and virulence.
595 Antimicrobial Agents and Chemotherapy **54**:2000–2009.

596 24. **Laubacher ME**, **Ades SE**. 2008. The Rcs phosphorelay is a cell envelope stress response
597 activated by peptidoglycan stress and contributes to intrinsic antibiotic resistance. J
598 Bacteriol **190**:2065–2074.

599 25. **Majdalani N**, **Gottesman S**. 2005. The Rcs phosphorelay: a complex signal transduction
600 system. Annu Rev Microbiol **59**:379–405.

601 26. **Clarke DJ**. 2010. The Rcs phosphorelay: more than just a two-component pathway.
602 Future Microbiology **5**:1173–1184.

603 27. **Howery KE**, **Clemmer KM**, **Şimşek E**, **Kim M**, **Rather PN**. 2015. Regulation of the
604 Min cell division inhibition complex by the Rcs Phosphorelay in *Proteus mirabilis*. J
605 Bacteriol **197**:2499–2507.

606 28. **Howery KE**, **Clemmer KM**, **Rather PN**. 2016. The Rcs regulon in *Proteus mirabilis*:
607 Implications for motility, biofilm formation, and virulence. Curr Genet.

608 29. **Ranjit DK**, **Young KD**. 2013. The Rcs stress response and accessory envelope proteins
609 are required for *de novo* generation of cell shape in *Escherichia coli*. J Bacteriol
610 **195**:2452–2462.

611 30. **Meier-Dieter U**, **Starman R**, **Barr K**, **Mayer H**, **Rick PD**. 1990. Biosynthesis of
612 enterobacterial common antigen in *Escherichia coli*. Biochemical characterization of Tn10
613 insertion mutants defective in enterobacterial common antigen synthesis. J Biol Chem
614 **265**:13490–13497.

615 31. **Kuhn HM**, **Neter E**, **Mayer H**. 1983. Modification of the lipid moiety of the
616 enterobacterial common antigen by the "*Pseudomonas* factor". Infect Immun **40**:696–700.

617 32. **Kiss P**, **Rinno J**, **Schmidt G**, **Mayer H**. 1978. Structural studies on the immunogenic
618 form of the enterobacterial common antigen. Eur J Biochem **88**:211–218.

619 33. **Dell A**, **Oates J**, **Lugowski C**, **Romanowska E**, **Kenne L**, **Lindberg B**. 1984. The
620 enterobacterial common-antigen, a cyclic polysaccharide. Carbohydr Res **133**:95–104.

621 34. **Rick PD**, **Mayer H**, **Neumeyer BA**, **Wolski S**, **Bitter-Suermann D**. 1985. Biosynthesis
622 of enterobacterial common antigen. J Bacteriol **162**:494–503.

623 35. **Duda KA**, **Duda KT**, **Beczała A**, **Kasperkiewicz K**, **Radziejewska-Lebrecht J**,
624 **Skurnik M**. 2009. ECA-immunogenicity of *Proteus mirabilis* strains. Arch Immunol Ther
625 Exp **57**:147–151.

626 36. **Fomsgaard A**, **Freudenberg MA**, **Galanos C**. 1990. Modification of the silver staining
627 technique to detect lipopolysaccharide in polyacrylamide gels. Journal of Clinical
628 Microbiology **28**:2627–2631.

629 37. **Kunin CM**. 1963. Separation, characterization, and biological significance of a common
630 antigen in Enterobacteriaceae. J Exp Med **118**:565–586.

631 38. **Whang HY**, **Neter E**. 1962. Immunological studies of a heterogenetic enterobacterial
632 antigen (Kunin). J Bacteriol **84**:1245–1250.

633 39. **McCoy AJ**, **Liu H**, **Falla TJ**, **Gunn JS**. 2001. Identification of *Proteus mirabilis* mutants
634 with increased sensitivity to antimicrobial peptides. Antimicrobial Agents and
635 Chemotherapy **45**:2030–2037.

636 40. **Merritt ME**, **Donaldson JR**. 2009. Effect of bile salts on the DNA and membrane
637 integrity of enteric bacteria. Journal of Medical Microbiology **58**:1533–1541.

638 41. **Ramos-Morales F**, **Prieto AI**, **Beuzon CR**, **Holden DW**, **Casadesus J**. 2003. Role for
639 *Salmonella enterica* enterobacterial common antigen in bile resistance and virulence. J
640 Bacteriol **185**:5328–5332.

641 42. **Greenwood D**, **O'Grady F**. 1973. Comparison of the responses of *Escherichia coli* and
642 *Proteus mirabilis* to seven β-lactam antibiotics. Journal of Infectious Diseases.

643 43. **Claret L**, **Hughes C**. 2000. Functions of the subunits in the FlhD2C2 transcriptional
644 master regulator of bacterial flagellum biogenesis and swarming. Journal of Molecular
645 Biology **303**:467–478.

646 44. **Pearson MM**, **Yep A**, **Smith SN**, **Mobley HLT**. 2011. Transcriptome of *Proteus*
647 *mirabilis* in the murine urinary tract: virulence and nitrogen assimilation gene expression.
648 Infect Immun **79**:2619–2631.

649 45. **Engemann C**, **Kleber HP**. 2001. Epigenetic regulation of carnitine metabolising enzymes
650 in *Proteus* sp. under aerobic conditions. FEMS Microbiology Letters **196**:1–6.

651 46. **Eichler K**, **Buchet A**, **Lemke R**, **Kleber HP**, **Mandrand-Berthelot MA**. 1996.
652 Identification and characterization of the *caiF* gene encoding a potential transcriptional
653 activator of carnitine metabolism in *Escherichia coli*. J Bacteriol **178**:1248–1257.

654 47. **Landfald B**, **Strøm AR**. 1986. Choline-glycine betaine pathway confers a high level of
655 osmotic tolerance in *Escherichia coli*. J Bacteriol **165**:849–855.

656 48. **Beumer RR**, **Giffel Te MC**, **Cox LJ**, **Rombouts FM**, **Abee T**. 1994. Effect of exogenous
657 proline, betaine, and carnitine on growth of *Listeria monocytogenes* in a minimal medium.
658 Applied and Environmental Microbiology **60**:1359–1363.

659 49. **Kets E**, **Galinski EA**, **de Bont J**. 1995. Carnitine: a novel compatible solute in
660 *Lactobacillus plantarum* accumulated during osmotic stress.

661 50. **Xiao M**, **Lai Y**, **Sun J**, **Chen G**, **Yan A**. 2016. Transcriptional regulation of the outer
662 membrane porin gene *ompW* Reveals its physiological role during the transition from the
663 aerobic to the anaerobic lifestyle of *Escherichia coli*. Front Microbiol **7**:799.

664 51. **Bode NJ**, **Debnath I**, **Kuan L**, **Schulfer A**, **Ty M**, **Pearson MM**. 2015. Transcriptional
665 analysis of the MrpJ network: Modulation of diverse virulence-associated genes and direct
666 regulation of *mrp* fimbrial and *flhDC* flagellar operons in *Proteus mirabilis*. Infect Immun
667 **83**:2542–2556.

668 52. **Castelli ME**, **Fedrigo GV**, **Clementín AL**, **Ielmini MV**, **Feldman MF**, **García Véscovi**
669 **E**. 2008. Enterobacterial common antigen integrity is a checkpoint for flagellar biogenesis
670 in *Serratia marcescens*. J Bacteriol **190**:213–220.

671 53. **Furness RB**, **Fraser GM**, **Hay NA**, **Hughes C**. 1997. Negative feedback from a *Proteus*
672 class II flagellum export defect to the *flhDC* master operon controlling cell division and
673 flagellum assembly. J Bacteriol **179**:5585–5588.

674 54. **Yao Z**, **Kahne D**, **Kishony R**. 2012. Distinct single-cell morphological dynamics under
675 beta-lactam antibiotics. Molecular Cell **48**:705–712.

676 55. **Zupan JR**, **Cameron TA**, **Anderson-Furgeson J**, **Zambryski PC**. 2013. Dynamic FtsA
677 and FtsZ localization and outer membrane alterations during polar growth and cell
678 division in *Agrobacterium tumefaciens*. Proceedings of the National Academy of Sciences
679 **110**:9060–9065.

680 56. **Pannen D**, **Fabisch M**, **Gausling L**, **Schnetz K**. 2016. Interaction of the RcsB Response
681 regulator with auxiliary transcription regulators in *Escherichia coli*. Journal of Biological
682 Chemistry **291**:2357–2370.

683 57. **Belas R**, **Erskine D**, **Flaherty D**. 1991. Transposon mutagenesis in *Proteus mirabilis*. J
684 Bacteriol **173**:6289–6293.

685 58. **Kaniga K**, **Delor I**, **Cornelis GR**. 1991. A wide-host-range suicide vector for improving
686 reverse genetics in gram-negative bacteria: inactivation of the *blaA* gene of *Yersinia*
687 *enterocolitica*. Gene **109**:137–141.

688 59. **Zhang Y**, **Werling U**, **Edelmann W**. 2012. SLiCE: a novel bacterial cell extract-based
689 DNA cloning method. Nucleic Acids Research **40**:e55–e55.

690 60. **Guzman LM**, **Belin D**, **Carson MJ**, **Beckwith J**. 1995. Tight regulation, modulation, and
691 high-level expression by vectors containing the arabinose PBAD promoter. J Bacteriol
692 **177**:4121–4130.

693 61. **Saak CC**, **Gibbs KA**. 2016. The self-identity protein IdsD is communicated between cells
694 in swarming *Proteus mirabilis* colonies. J Bacteriol **198**:3278–3286.

695 62. **Gibbs KA**, **Urbanowski ML**, **Greenberg EP**. 2008. Genetic determinants of self identity
696 and social recognition in bacteria. Science **321**:256–259.

697 63. **Schindelin J**, **Arganda-Carreras I**, **Frise E**, **Kaynig V**, **Longair M**, **Pietzsch T**,
698 **Preibisch S**, **Rueden C**, **Saalfeld S**, **Schmid B**, **Tinevez J-Y**, **White DJ**, **Hartenstein V**,
699 **Eliceiri K**, **Tomancak P**, **Cardona A**. 2012. Fiji: an open-source platform for biological-
700 image analysis. Nat Methods **9**:676–682.

701 64. **Sambrook J**, **Russell DW**. 2006. Purification of nucleic acids by extraction with phenol:
702 chloroform. Cold Spring Harbor Protocols **2006**:pdb.prot4455.

703 65. **Kim D**, **Pertea G**, **Trapnell C**, **Pimentel H**, **Kelley R**, **Salzberg SL**. 2013. TopHat2:
704 accurate alignment of transcriptomes in the presence of insertions, deletions and gene
705 fusions. Genome Biol **14**:R36.

706 66. **Trapnell C**, **Hendrickson DG**, **Sauvageau M**, **Goff L**, **Rinn JL**, **Pachter L**. 2012.
707 Differential analysis of gene regulation at transcript resolution with RNA-seq. Nature
708 Biotechnology **31**:46–53.

709 67. **Tatusov RL**, **Galperin MY**, **Natale DA**, **Koonin EV**. 2000. The COG database: a tool
710 for genome-scale analysis of protein functions and evolution. Nucleic Acids Research
711 **28**:33–36.

712 68. **Kanehisa M**, **Sato Y**, **Kawashima M**, **Furumichi M**, **Tanabe M**. 2016. KEGG as a
713 reference resource for gene and protein annotation. Nucleic Acids Research **44**:D457–62.

714

715 **Figure Legends**

716 **Figure 1: Loss of *rffG* affects OM structures and cell envelope integrity**

717 A. Silver-stained LPS extracted surface-grown WT, Δ*rffG*, and *rffG*-complemented populations.

718 LPS-associated moieties are labeled on the left.

719 B. Cultures of the WT, Δ*rffG,* and *rffG*-complemented strains were normalized based on OD_{600},

720 and 10-fold serial dilutions were spotted on indicated % bile salt media. Images are

721 representative, n = 3.

722 C. WT and Δ*rffG* strains were spread onto swarm-permissive agar pads containing 0 or 10

723 µg/mL Cb. Shown are cells after one, two, or four hours of incubation on a surface. Images are

724 representative; n =3. Scale bars = 10 µm.

725

726 **Figure 2: Loss of *rffG* inhibits swarmer cell elongation and swarm motility**

727 A. WT and Δ*rffG* strains were grown on swarm-permissive medium, on which cells engage in

728 the swarm cycle (see 2B) and remain along the top of the surface.

729 B. Cartoon depictions of the morphological state of cells grown on swarm permissive solid

730 medium. On surfaces, cells elongate up to 40-fold before engaging in motility and dividing into

731 short (1-2 µm) rigid rods.

732 C. Phase contrast and epifluorescence microscopy of WT, Δ*rffG*, or *rffG*-complemented

733 populations after two, four, and six hours on a swarm-permissive surface. Strains carried either

734 an empty vector or expression vector to allow growth on selective medium. Venus fluorescence

735 corresponds to *fliA* reporter expression and is shown for the six-hour time point. Rolling ball

736 background subtraction was performed using FIJI (63). Magenta arrow highlights an elongating

737 cell in the Δ*rffG* population that is bulging. Frames from a time-lapse of such cells bulging are in
738 Figure SF2. Scale bars = 10 µm.
739
740 **Figure 3: The expression profile of Δ*rffG* cells is distinct from that of WT on surfaces**
741 A. Graphical summary of genes differentially regulated in Δ*rffG* versus short, non-motile WT
742 cells grown on a swarm-permissive surface. The x-axis corresponds to each gene on the *P.*
743 *mirabilis* strain BB2000 chromosome. The y-axis corresponds to a $\log_2$-fold difference in gene
744 expression. All data are shown. Red circles indicate genes that are also regulated by RcsB as
745 determined in (27, 28). The most highly altered gene (*mrpA* at ~ 200-fold) is labeled.
746 B. Summary of the COG functional categories (67) for the significant differentially regulated
747 genes.
748
749 **Figure 4: RcsB and FlhDC rescue swarm elongation of *rffG*-deficient cells; RcsB is**
750 **additionally essential for maintaining cell shape**
751 Epifluorescence microscopy of (A) WT + *flhDC*, (B) Δ*rffG* + *flhDC*, (C) Δ*rcsB*, and (D)
752 Δ*rffG*Δ*rcsB* populations; all strains carry the chromosomal *fliA* reporter. Images were taken once
753 swarm motility initiated (~4-6 hours on surface). Rolling ball background subtraction on *fliA*
754 reporter images was conducted using FIJI (63). Magenta arrows indicate a cell exhibiting shape
755 and polarity defects. Left, phase contrast; middle, membrane stain; right, Venus expression.
756 Scale bars = 10 µm.
757
758 **Figure 5: Rcs activation inhibits cell elongation while maintaining cell envelope integrity.**

759 Activation of the Rcs phosphorelay results in activation of adherence-promoting genes when the
760 membrane is compromised. We hypothesize that artificial, constitutive expression of *flhDC*
761 under the *lac* promoter can uncouple Rcs repression of *flhDC* from activation these pathways,
762 thereby allowing full rescue of Δ*rffG* swarmer cell elongation through constitutive expression of
763 *flhDC*.
764
765

766 **Strain Table**

Name	**Description**	**Source**
WT	Wild type strain	(57)
Δ*rffG*	BB2000Δ*rffG::CmR*	This study
Δ*rcsB*	BB2000Δ*rcsB*	This study
Δ*rffG* complemented	BB2000Δ*rffG/*pBBR1-P(*lac*)-*rffG*	This study
WT + *flhDC*	BB2000/pBBR1-P(*lac*)-*flhDC*	This study
Δ*rffG* + *flhDC*	BB2000Δ*rffG/*pBBR1-P(*lac*)-*flhDC*	This study
Δ*rffG*Δ*rcsB*	BB2000Δ*rcsB*Δ*rffG::CmR*	This study
WT::*fliA, Venus*	BB2000 with ribosomal binding site (RBS) and Venus inserted immediately downstream of *fliA* stop codon	This study; Venus construct from P. Cluzel
WT::*fliA, Venus* + *flhDC*	WT::*fliA, Venus*/pBBR1-P(*lac*)-*flhDC*	This study
Δ*rffG::fliA, Venus*	Δ*rffG* with (RBS) and Venus inserted immediately downstream of *fliA* stop codon	This study

Δ*rffG*::*fliA, Venus* + *flhDC*	Δ*rffG*::*fliA, Venus*/pBBR1-P(*lac*)-*flhDC*	This study
Δ*rcsB*::*fliA, Venus*	Δ*rcsB* with (RBS) and Venus inserted immediately downstream of *fliA* stop codon	This study
Δ*rffG*Δ*rcsB*::*fliA, Venus*	Δ*rffG*Δ*rcsB* with (RBS) and Venus inserted immediately downstream of *fliA* stop codon	This study
WT + empty vector	BB2000/pBBR1-NheI	This study
Δ*rffG* + empty vector	BB2000Δ*rffG*::*CmR*/pBBR1-NheI	This study

767
768

769 **Plasmid Table**

Name	**Descriptions**	**Source**
empty vector	pBBR1-NheI	(62)
+ *rffG*	pBBR1-P(lac)-r*ffG*	This study
+ *flhDC*	pBBR1-Pr(lac)-*flhDC*	This study

770
771

772

773 **Table 1: Top 20 genes up-regulated in Δ*rffG* relative to WT**

Transcript	**Product**	**Fold Change**	**Rcs Regulon?***
mrpA	major mannose-resistant/Proteus-like fimbrial protein	200.27	Yes
caiF	DNA-binding transcriptional activator CaiF	63.60	
pmpA	fimbrial subunit	55.46	
BB2000_1924	transcriptional regulator	45.63	
BB2000_1499	fimbrial subunit	44.85	
BB2000_3017	fimbrial operon regulator	44.59	
zntB	zinc transporter	42.83	
mrpG	fimbrial subunit	42.72	
BB2000_0667	hypothetical protein		
ompW	outer membrane protein W	33.70	
BB2000_2725	TetR-family transcriptional regulator	32.64	
dcuB	anaerobic C4-dicarboxylate transporter	29.58	
BB2000_0531	sigma 54 modulation protein	25.53	

BB2000_0331	heat shock protein HtpX	22.81	
BB2000_0299	hypothetical protein	22.47	
BB2000_0395	hypothetical protein	21.42	Yes
BB2000_0229	hypothetical protein	21.19	
BB2000_1497	fimbrial chaperone protein	20.97	
mrpJ	fimbrial operon regulator	19.08	
dmsA	dimethyl sulfoxide reductase chain A	18.99	Yes

774
775

776 * Based on the published RcsB regulon in *P. mirabilis* (27, 28)

777

778

779 **Table 2: Top 20 genes down-regulated in Δ*rffG* relative to WT**

Transcript	**Product**	**Fold Change**	**Rcs Regulon?***
cspB	cold shock protein	0.01	
flgN	flagella synthesis protein	0.03	
BB2000_1016, BB2000_1017	cold shock protein, heat shock protein	0.04	
flgM	anti-sigma28 factor FlgM	0.04	
BB2000_3499	lipoprotein	0.05	Yes
fliE	flagellar hook-basal body complex protein	0.05	
BB2000_1271	putative MFS-type transporter YdeE	0.07	
fliA	flagellar biosynthesis sigma factor	0.08	Yes
BB2000_1466	hypothetical protein		Yes
holD	DNA polymerase III subunit psi	0.10	Yes
intB	prophage integrase	0.11	
fliM, fliN	flagellar motor switch protein FliM, flagellar motor switch protein FliN	0.11	Yes
BB2000_0342	transcriptional regulator	0.11	Yes

BB2000_0996, umoD	hypothetical protein, exported protein (upregulator of flagellar master operon)	0.12	Yes
rpsO	30S ribosomal protein S15	0.12	
ccm	membrane protein (Ccm1 protein)	0.12	Yes
rplI	50S ribosomal protein L9	0.12	
fliZ	flagella biosynthesis protein FliZ	0.12	Yes
BB2000_2557	phospholipid-binding protein	0.13	Yes
BB2000_2289, fruK	hypothetical protein, 1-phosphofructokinase	0.13	

780
781

782 * Based on the published RcsB regulon in *P. mirabilis* (27, 28)

783

784

785

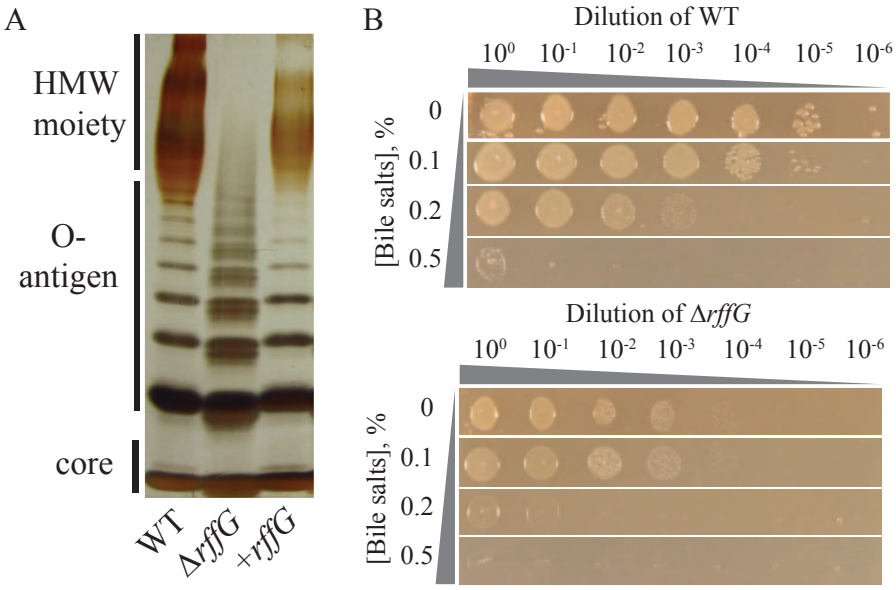

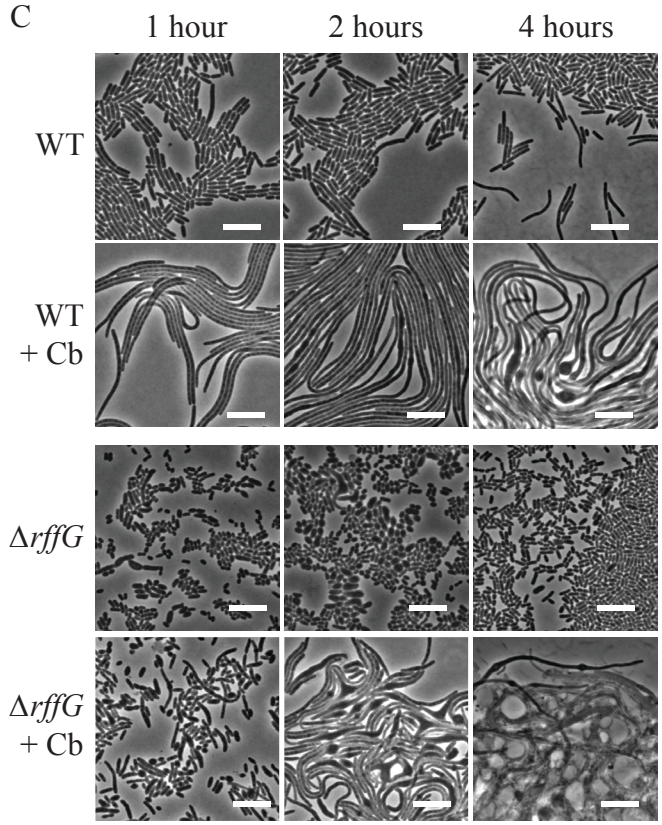

Legend:

Figure 1: Loss of *rffG* affects OM structures and cell envelope integrity

A. Silver-stained LPS extracted surface-grown WT, Δ *rffG*, and *rffG*-complemented populations. LPS-associated moieties are labeled on the left.

B. Cultures of the WT, Δ*rffG*, and *rffG*-complemented strains were normalized based on OD_{600}, and 10-fold serial dilutions were spotted on non-swarm permissive medium with indicated % bile salt media. Images are representative, n = 3.

C. WT and Δ*rffG* strains were spread onto swarm-permissive agar pads containing 0 or 10 µg/mL Cb. Shown are cells after one, two, or four hours of incubation on a surface. Images are representative, n =3. Scale bars = 10 µm.

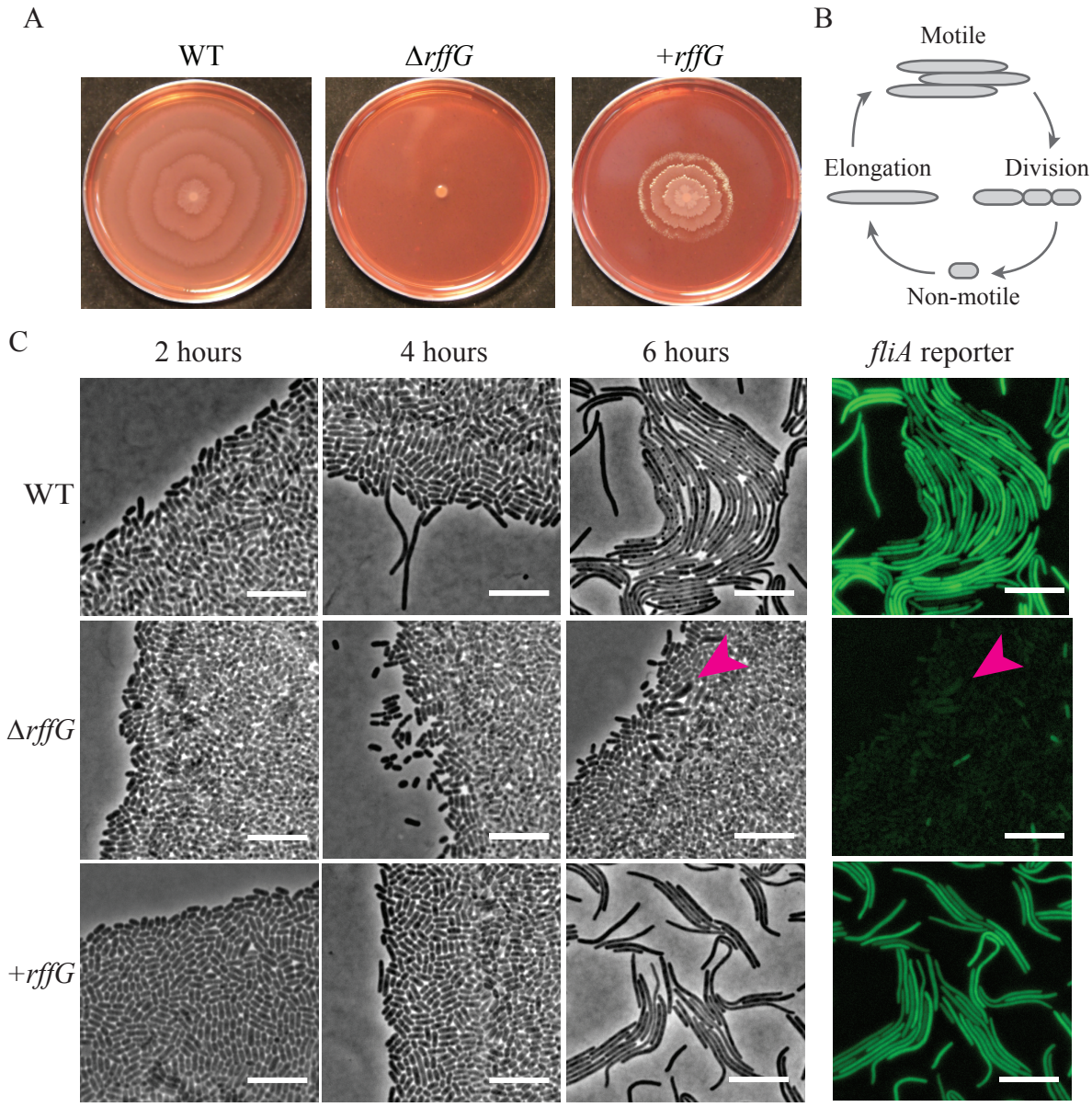

Legend:

Figure 2: Loss of *rffG* inhibits swarmer cell elongation and swarm motility

A. WT and Δ*rffG* strains were grown on swarm-permissive medium, on which cells engage in the swarm cycle (see 2C) and remain along the top of the surface.

B. Cartoon depictions of the morphological state of cells grown on swarm permissive media. On surfaces, cells elongate up to 40-fold before engaging in motility and dividing into short (1-2 µm) rigid rods.

C. Phase contrast and epifluorescence microscopy of WT, Δ*rffG*, or *rffG*-complemented populations after two, four, and six hours on a swarm-permissive surface. Strains carried either an empty vector or expression vector to allow growth on selective medium. Venus fluorescence corresponds to *fliA* reporter expression and is shown for the six-hour time point. Rolling ball background subtraction was performed using FIJI (61). Magenta arrow highlights an elongating cell in the Δ*rffG* population that is bulging. Frames from a time-lapse of such cells bulging are in Figure SF2. Scale bars = 10 µm.

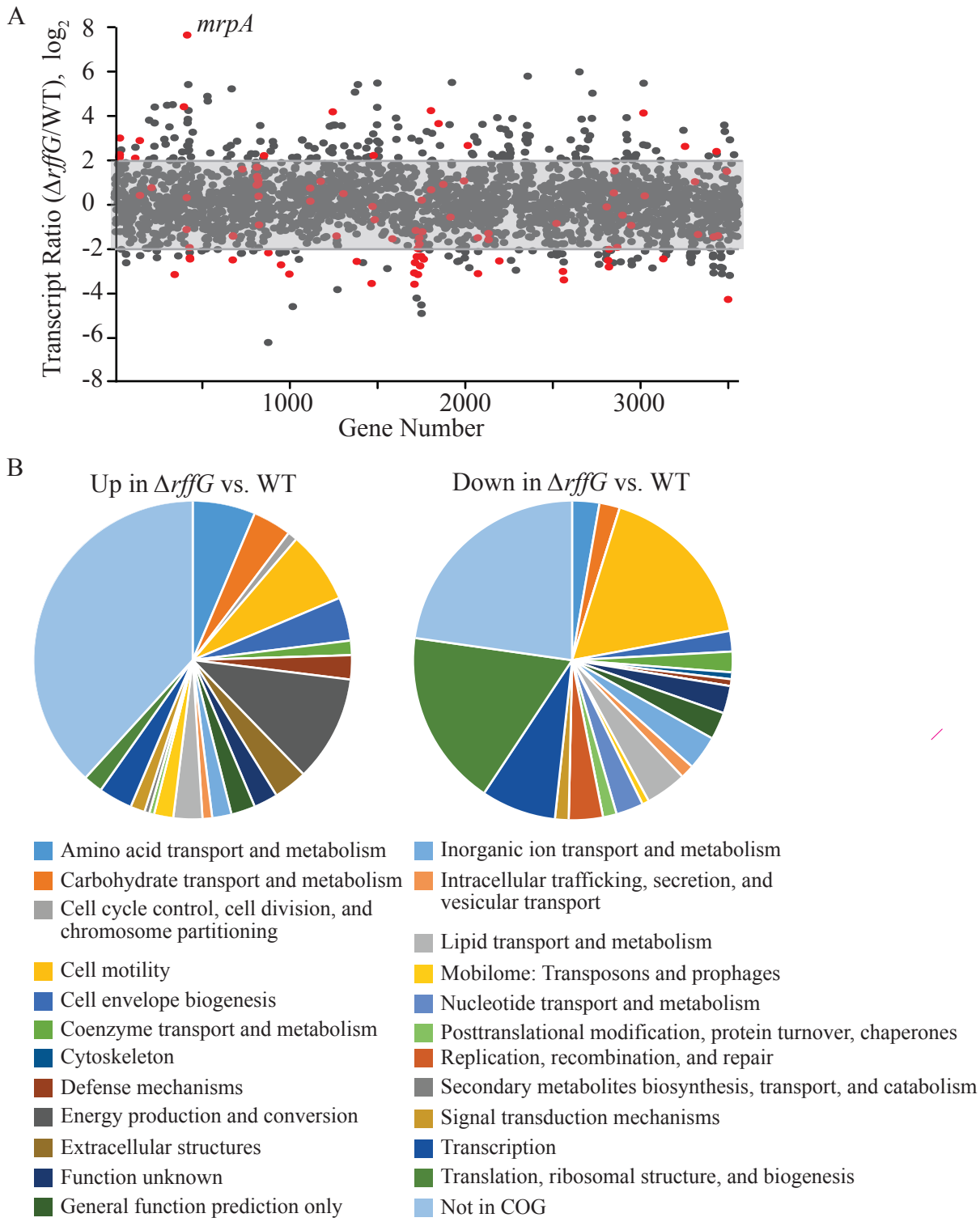

Legend:

Figure 3: The expression profile of ΔrffG cells is distinct from that of WT on surfaces

A. Graphical summary of genes differentially regulated in Δ*rffG* versus short, non-motile WT cells grown on a swarm-permissive surface. The x-axis corresponds to each gene on the *P. mirabilis* strain BB2000 chromosome. The y-axis corresponds to a log2-fold difference in gene expression. All data are shown. Red circles indicate genes that are also regulated by RcsB as determined in (30). The most highly altered gene (*mrpA* at ~ 200-fold) is labeled.

B. Summary of the COG functional categories for the significant differentially regulated genes (65).

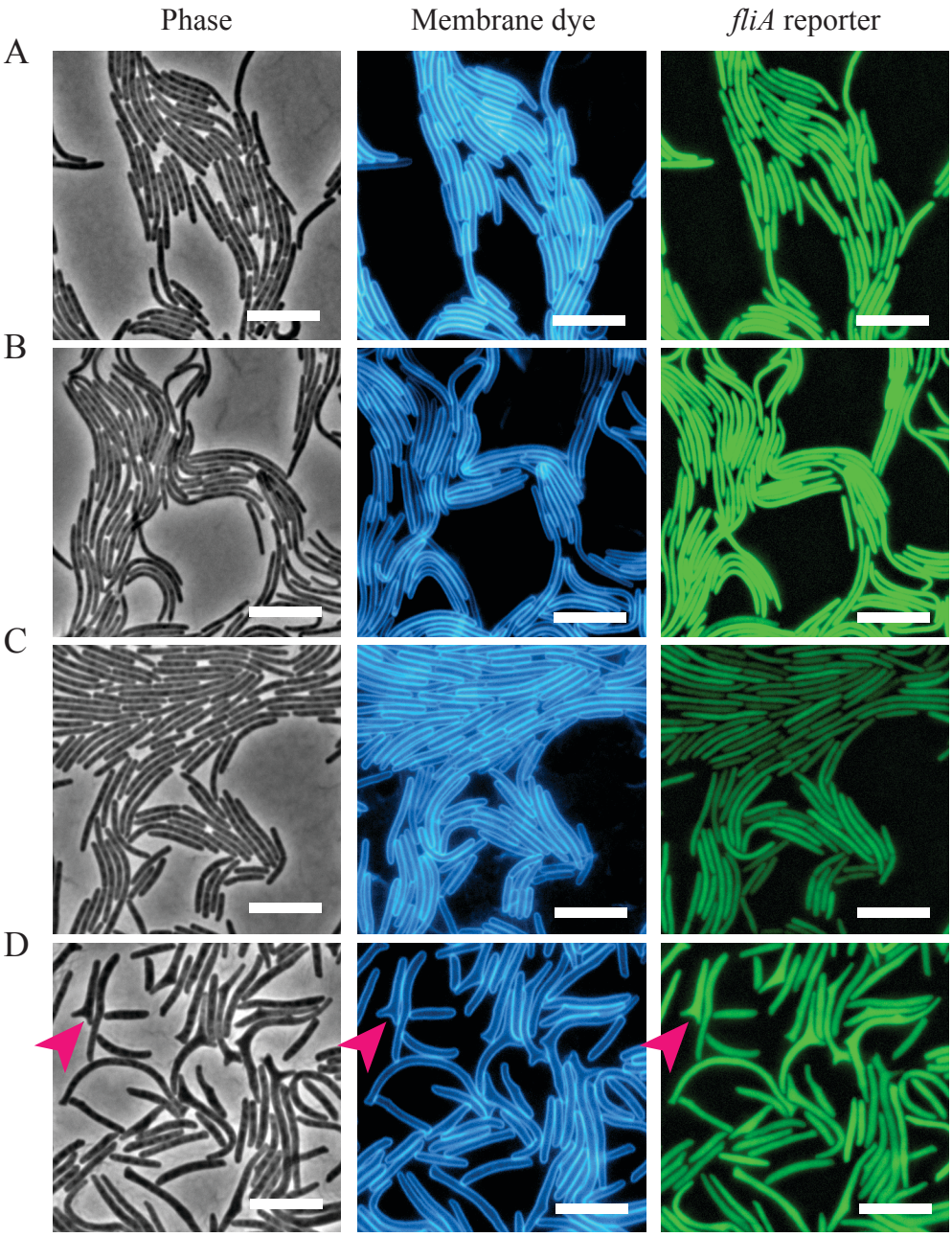

Legend:

Figure 4: RcsB and FlhDC rescue swarm elongation of *rffG*-deficient cells; RcsB is additionally essential for maintaining cell shape

Epifluorescence microscopy of (A) WT + *flhDC*, (B) Δ*rffG* + *flhDC*, (C) Δ*rcsB*, and (D) Δ*rffG*Δ*rcsB* populations; all strains carry the chromosomal *fliA* reporter. Images were taken once swarm motility initiated (~4-6 hours on surface). Rolling ball background subtraction on fliA reporter images was conducted using FIJI (61). Left, phase contrast; middle, membrane stain; right, Venus expression. Scale bars = 10 µm.

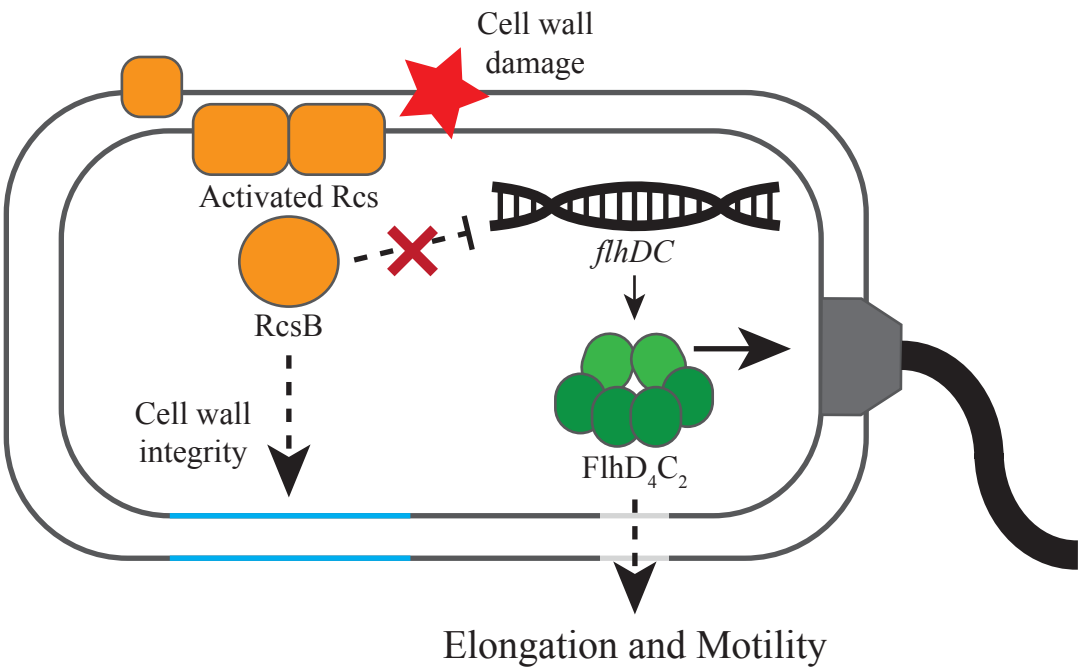

Legend:
Figure 5: Rcs activation inhibits cell elongation while maintaining cell envelope integrity. We hypothesize that activation of the Rcs phosphorelay results in activation of cell envelope-protective pathways during times of stress. We posit that artificial expression of *flhDC* under the lac promoter uncouples Rcs repression of *flhDC* from activation these protective pathways, thereby allowing full rescue of Δ*rffG* swarmer cell elongation through constitutive expression of *flhDC*.